# Effect of microscopic temperature–dependent binding energies in the decay of $^{32}$Si$^*$ nuclear system

*Manpreet Kaur*



*Institute of Physics*
*Bhubaneswar*

**International Conference on Nuclear Structure Properties**

Selcuk University, Turkey

02–04 June, 2021

# CONTENTS

- Motivation

- Methodology

- Results & discussion

- Conclusion

# Motivation

➢ The investigation of fusion reactions involving light neutron-rich exotic nuclei is of paramount significance to understand nucleosynthesis in astrophysical scenarios.

➢ Recently, $^{20}O+^{12}C$ reaction has been studied with measurement of fusion cross-section ($\sigma_{fus}$) *[M. J. Rudolph et al., PRC 85, 024605 (2012)]*. Bass model under predicts the $\sigma_{fus}$ and time-dependent Hartree-Fock model also fails to explain the experimental data.

➢ To explicate the same, the investigation of $^{20}O+^{12}C$ reaction at near barrier energies has been made within quantum mechanical fragmentation theory (QMFT) based dynamical cluster-decay model (DCM).

➢ The T-dependent binding energies (T.B.E.) are one of the fundamental ingredient of the DCM. So far, the T.B.E. of Davidson formula *[N. J. Davidson, NPA 570, 61c (1994)]* together with the shell corrections by Myers-Swiatecki *[W. D. Myers, NPA 81, 1 (1966)]* have been used within DCM.

# Motivation

➢ It is important to point out that the masses of known regimes at T = 0 MeV have been employed in the fitting of different mass formulae and good agreement with experimental data is anticipated in these regions.

➢ The divergence in the unknown regions where no common trend or correlation is seen taking one of the mass formula as a reference case *[W. Mitting, Europhys. News 35, no. 4 (2004)*; arXiv:nuclth/ 0504063]. Therefore, any mass formula cannot be used as a reliable guide to get T.B.E.

➢ We have addressed this issue by inculcation of T.B.E. from the microscopic relativistic mean field theory (RMFT) within DCM.

➢ Here, nuclear properties such as binding energies etc. of only a few doubly magic nuclei are fitted at $T = 0$ with ref to explt. data and predictions made for other thousands of nuclei are in consonance with experimental data. Hence, the prediction of T.B.E. by RMF theory is reliable.

➢ It is important to explore the role of microscopic T.B.E. upon fragmentation process and different variables involved in the fusion cross-section estimation.

# Methodology

# Quantum Mechanical Fragmentation Theory (QMFT)

➢ The QMFT [R. K. Gupta, W. Scheid, and W. Greiner, PRL **35**, 353 (1975); PRL **32**, 548 (1974)] is a unified description of two body channels in both fusion and fission processes.

➢ In QMFT, nuclear dynamics is explained by the mass parameters defining the kinetic energy of the system while the static properties of nuclear system are determined by the potential energy surfaces.

➢ This theory is based on the fact that the fragments are pre-born prior to the decay of the nucleus. Once the clusters are formed, their penetration probability P across the interaction barrier can be calculated by using the WKB approximation.

❖ *In QMFT based DCM, the decay of an excited compound nucleus (CN) is studied as a collective clusterization process for emissions of the LPs (A≤4), as well as the IMFs (5 ≤ A ≤ 20) and FF, in contrast to the statistical models in which each type of emission is treated on different footing.*

# Dynamical Cluster-decay Model (DCM)

*The decay of excited compound system is worked out in terms of collective coordinates of QMFT as:*

| Relative separation coordinate $R$ | Deformation $\beta_{\lambda i}$, orientations $\theta_i$ of two nuclei | Mass asymmetry coordinate $\eta = (A_1-A_2)/(A_1+A_2)$ |
|---|---|---|

In terms of these collective coordinates using the partial wave analysis, for hot and rotating ($T \neq 0$ and $l \neq 0$) CN, the decay cross-section is defined as

$$\sigma = \frac{\pi}{k^2} \sum_{\ell=0}^{\ell_{ai}/\ell_{max}} (2\ell+1) P_0 P \qquad k = \sqrt{\frac{2\mu E_{c.m.}}{\hbar^2}}$$

**Preformation probability ($P_0$)**

$$P_0 = |\psi(\eta(A_i))|^2 \sqrt{B_{\eta\eta}} \frac{2}{A_{CN}}$$

**Penetrability (P)**

$$P = \exp\left[ -\frac{2}{\hbar} \int_{R_a}^{R_b} \{2\mu [V(R, T) - V(Ra, T)]\} dR \right]$$

**Schrodinger Eq.**

$$-\frac{\hbar^2}{2\sqrt{B_{\eta\eta}}} \frac{\partial}{\partial \eta} \frac{1}{\sqrt{B_{\eta\eta}}} \frac{\partial}{\partial \eta} + V_R(\eta, T) \psi_R^{(v)}(\eta) = E_R^{(v)} \psi_R^{(v)}(\eta)$$

**Fragmentation potential**

$$V_R(\eta, T) = \sum_{i=1}^{2} [V_{LDM}(A_i, Z_i, T)] + \sum_{i=1}^{2} [\delta U_i] \exp(-T^2/T_0^2) + V_C(\eta, R, \beta_{\lambda i}, \theta_i, \ell, T)$$
$$+ V_P(\eta, R, \beta_{\lambda i}, \theta_i, \ell, T) + V_\ell(\eta, R, \beta_{\lambda i}, \theta_i, \ell, T)$$

**T-dependent RMFT B.E.**

# Relativistic Mean Field (RMF) Model

Lagrangian for nucleon-meson many body system [J. Boguta et al., NPA 292, 413 (1977)]

$$\mathcal{L} = \overline{\psi}\{i\gamma^\mu \partial_\mu - M\}\psi + \frac{1}{2}\partial^\mu \sigma \partial_\mu \sigma - \frac{1}{2}m_\sigma^2 \sigma^2 - \frac{1}{3}g_2\sigma^3 - \frac{1}{4}g_3\sigma^4 - g_s\overline{\psi}\psi\sigma + \frac{1}{2}m_w^2 \omega^\mu \omega_\mu - g_\omega \overline{\psi}\gamma^\mu \psi \omega_\mu$$

$$- \frac{1}{4}\Omega^{\mu\nu}\Omega_{\mu\nu} + \frac{1}{2}m_\rho^2 \vec{R}^\mu . \vec{R}_\mu - g_\rho \overline{\psi}\gamma^\mu \vec{\tau}\psi . \vec{R}^\mu - \frac{1}{4}\vec{R}^{\mu\nu}.\vec{R}_{\mu\nu} - e\overline{\psi}\gamma^\mu \frac{(1-\tau_3)}{2}\psi A_\mu - \frac{1}{4}F^{\mu\nu}F_{\mu\nu}.$$

## Equations of motion

$$\left(-i\alpha.\triangledown + \beta(M + g_\sigma\sigma) + g_\omega\omega + g_\rho\tau_3\rho_3\right)\psi_i = \varepsilon_i\psi_i,$$

$$(-\triangledown^2 + m_\sigma^2)\sigma(r) = -g_\sigma\rho_s(r) - g_2\sigma^2 - g_3\sigma^3,$$

$$(-\triangledown^2 + m_\omega^2)V(r) = g_\omega\rho(r),$$

$$(-\triangledown^2 + m_\rho^2)R(r) = g_\rho\rho_3(r),$$

$$-\triangledown^2 A_0(r) = e\rho_c(r).$$

## Densities

$$\rho(r) = \sum_i n_i \, \psi_i^\dagger(r)\,\psi_i(r),$$

$$\rho_s(r) = \sum_i n_i \, \psi_i^\dagger(r)\,\gamma_0\,\psi_i(r),$$

$$\rho_3(r) = \sum_i n_i \, \psi_i^\dagger(r)\,\tau_3\,\psi_i(r),$$

$$\rho_c(r) = \sum_i n_i \, \psi_i^\dagger(r)\left(\frac{1-\tau_3}{2}\right)\psi_i(r).$$

$$n_i = v_i^2 = \frac{1}{2}\left[1 - \frac{\epsilon_i - \lambda}{\tilde{\epsilon}_i}[1 - 2f(\tilde{\epsilon}_i, T)]\right].$$

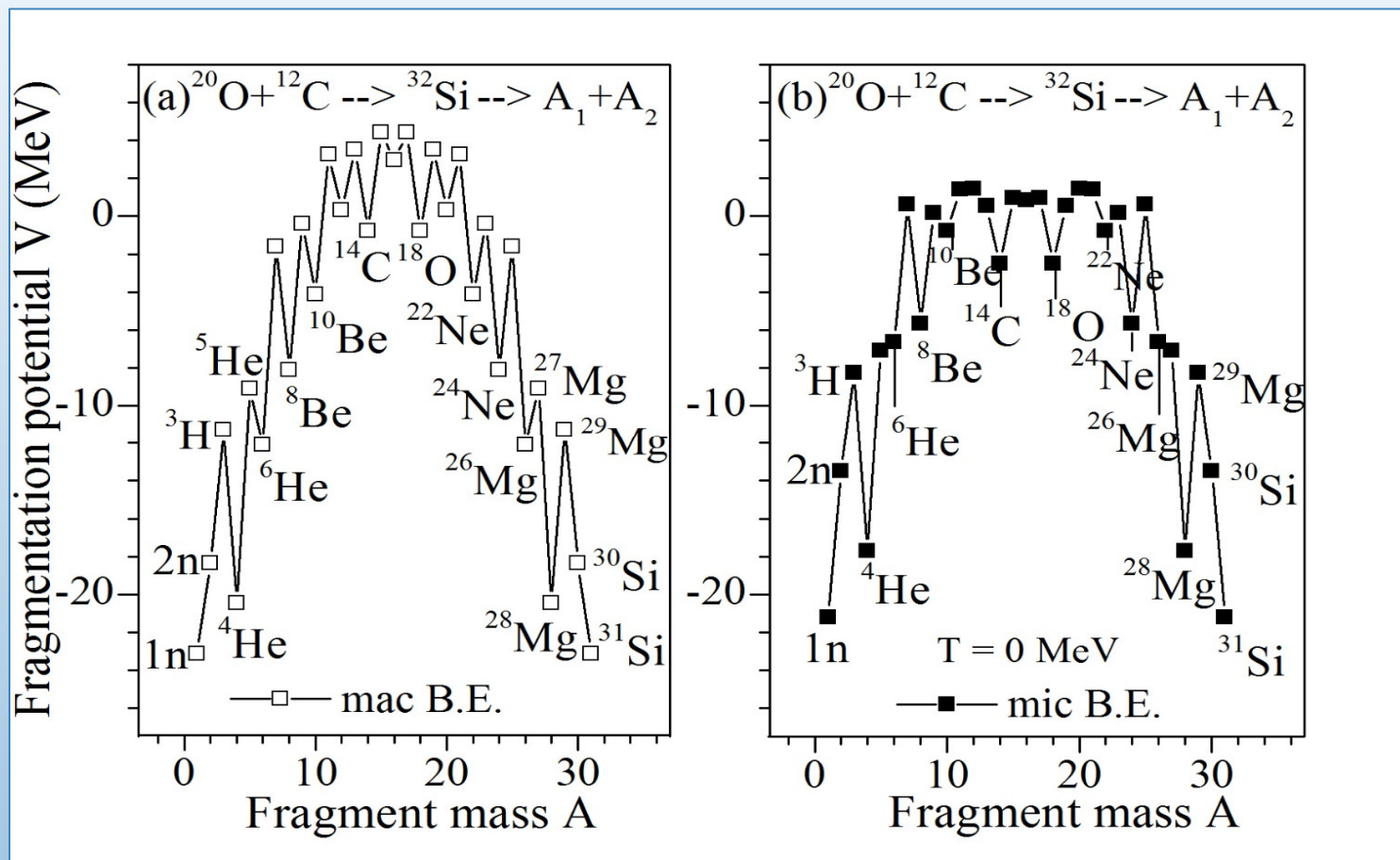$$f(\tilde{\epsilon}_i, T) = \frac{1}{(1 + exp[\tilde{\epsilon}_i/T])}$$

# Results and discussion



FIG. 1. Frag. potential in the decay of $^{32}$Si at $T = 0$ MeV using (a) Davidson formula-based macroscopic (mac) B.E. and (b) RMF theory-based microscopic (mic) B.E.

❖ The structure of fragmentation potential and minimized/favored fragments essentially remains unchanged with a small change in the magnitude for mac and mic B.E. cases.
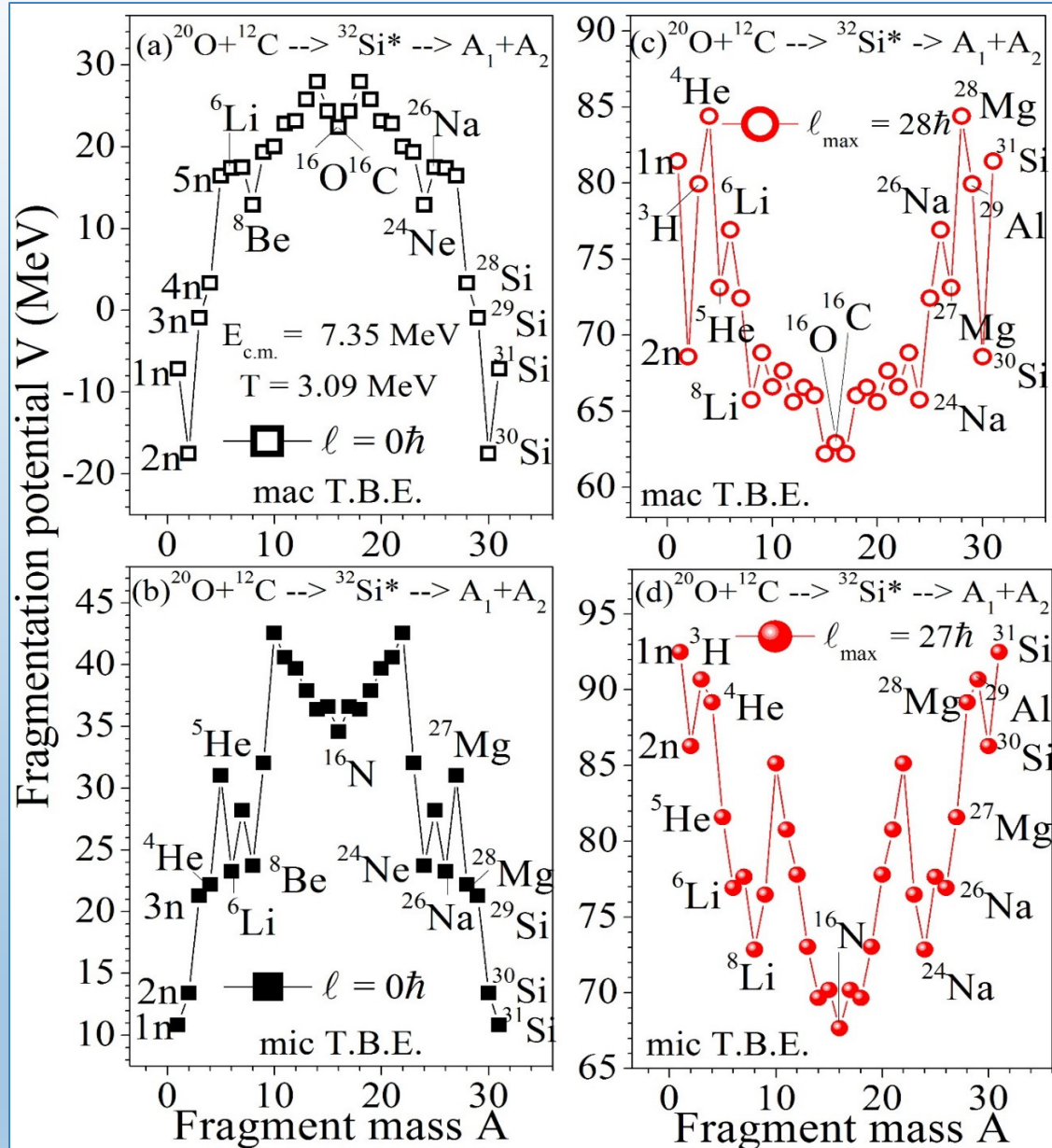
FIG. 2. Mass-dependence of frag. potential in the decay of $^{32}$Si* formed at $T = 3.09$ MeV using (a, c) macroscopic T.B.E. and (b, d) microscopic T.B.E.

➢ For mac T.B.E. case, the neutrons (1n-5n) are the most probable exit channels.

➢ However, for mic T.B.E. case, in addition to neutron channels, the $\alpha$ channels ($^4$He, $^5$He) also come into the picture.

➢ A higher value of fragmentation potential for LP for the mic T.B.E. case than the mac T.B.E.

➢ The structure of symmetric mass fragments (SMF) gets changed with inculcation of mic T.B.E.

➢ The shape of potential energy surface changes significantly for LP and SMF window ($A/2 \pm 5$) for mic T.B.E. case.
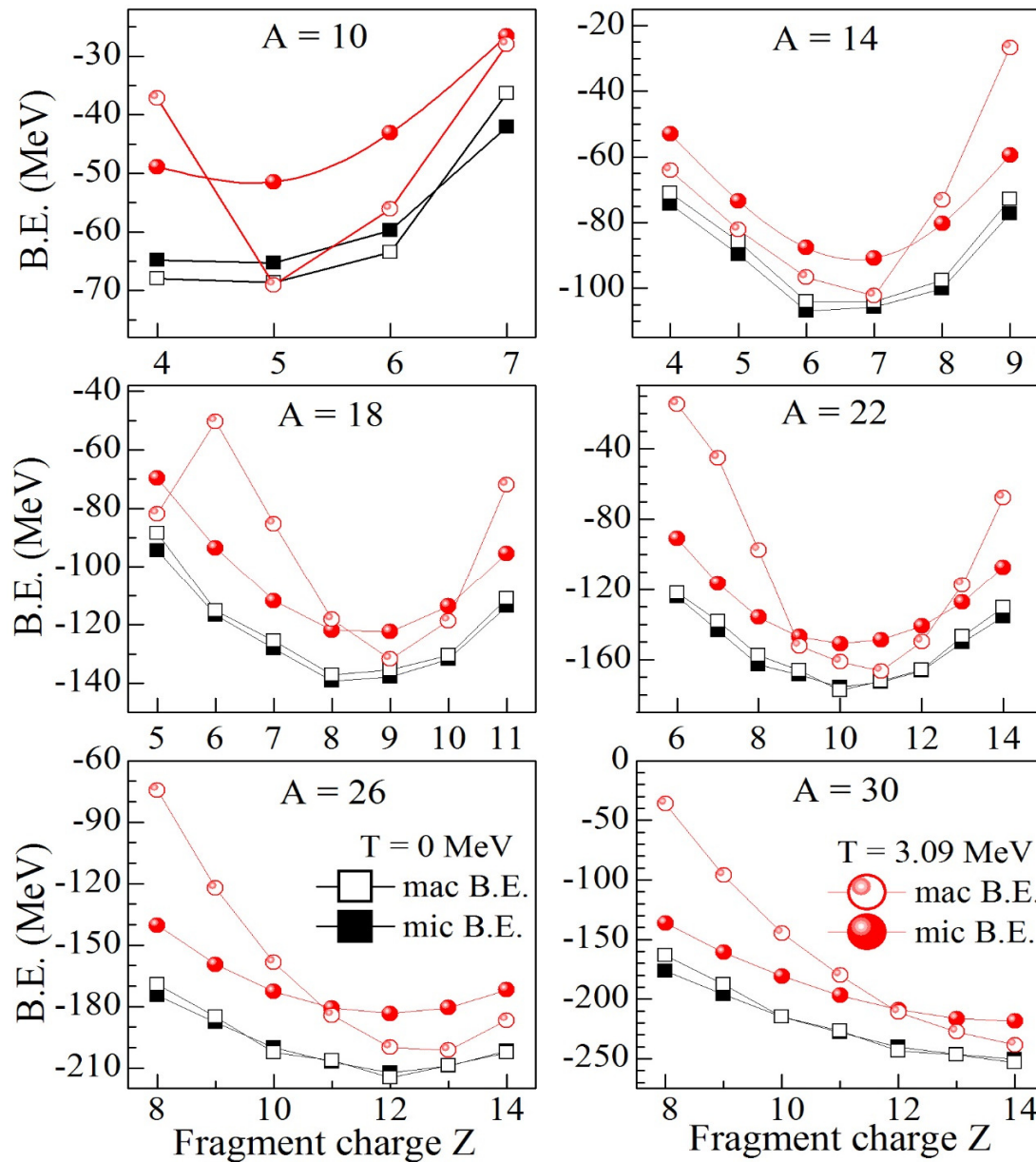
FIG. 3. The macroscopic and microscopic B.E. for some isobars with mass number $A = 10, 14, 18, 22, 26, 30$ at $T = 0$ MeV and 3.09 MeV

➤ At T = 3.09 MeV, the magnitude as well as the shape of binding energy parabola is quite different for theory and mass formula computed T.B.E.

➤ Davidson formula based mac B.E. are calculated via empirical fitting of constants in reference to explt. data at T = 0.

➤ Large diversion in the predictions of different mass formulas in the unknown regimes (Fig. 4 of Europhysics News Vol. 35, No. 4 (2004)), where experimental data is unavailable, with reference to some mass formula [arXiv:nuclth/0504063]. It raises the question about the predictive efficacy of mass formulas.
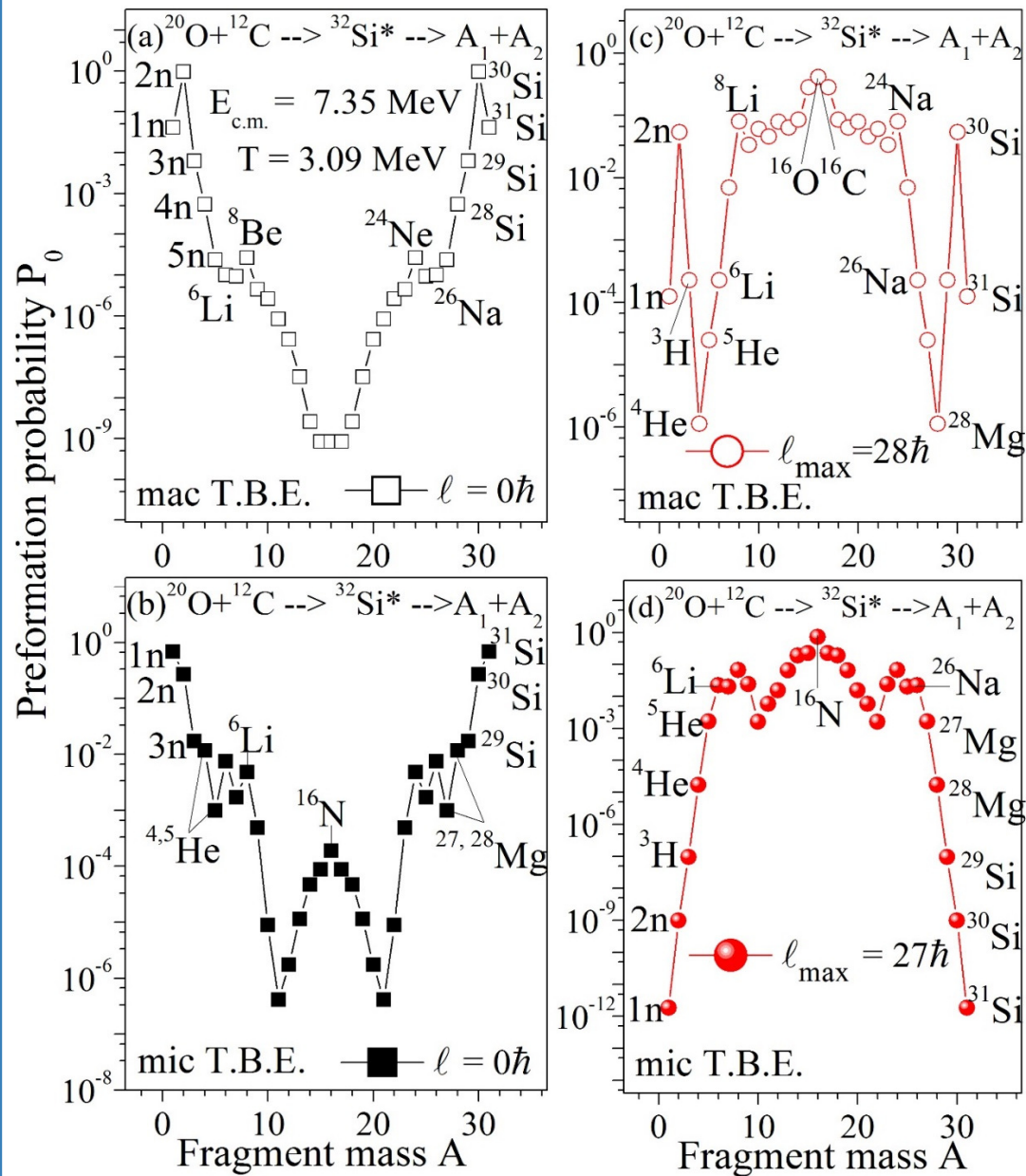
FIG. 4. Preformation prob. $P_0$ in the decay of $^{32}$Si* formed at $T = 3.09$ MeV using (a, c) macroscopic T.B.E. and (b, d) microscopic T.B.E.

- The fragmentation potential being an essential input in the $P_0$ calculations, encompass the nuclear structure imprints in the $P0$ of different fragments.

- The preformation profile evolves from asymmetric (Fig. (a, b)) to symmetric (Fig. (c, d)) one while moving from lower to higher $\ell$-value for both cases of T.B.E.

- $P_0$ value of alpha channels ($^{4,5}$He) is more for mic T.B.E. case (Fig. (d)) compared to mac T.B.E case.

- The shape of preformation profile changes notably for light particles and SMF window by consideration of mic T.B.E
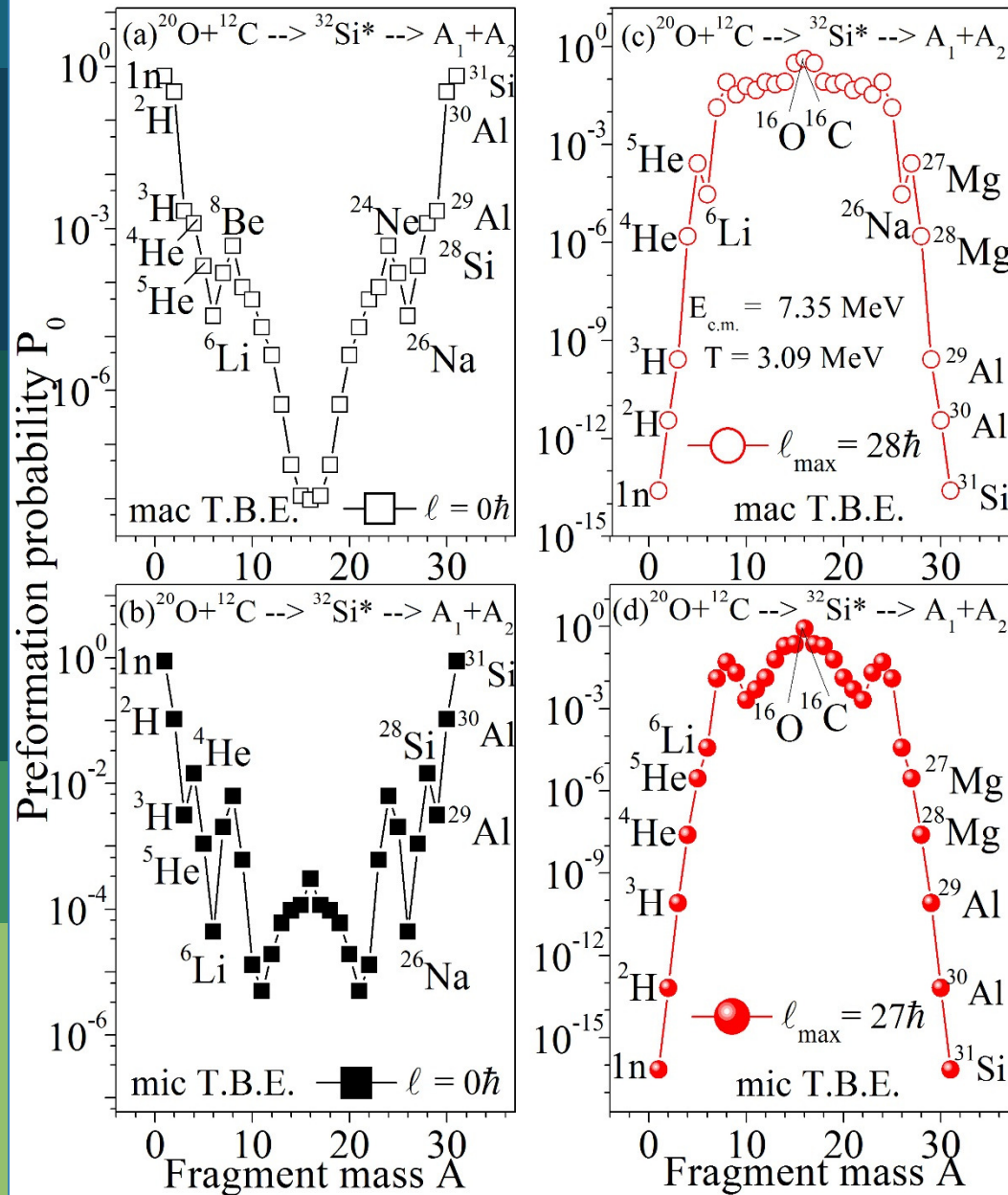
FIG. 5. Same as Fig. 4 but for replaced LCP

➢ It is important to note that experimentally measured fusion cross-section involve contributions of LCP (Z ≤ 2, 2 ≤ A ≤ 6) only [*M. J. Rudolph et al., PRC* **85**, *024605 (2012)*], therefore fusion cross-section is evaluated by addition of contribution of each LCP channel.

➢ To calculate fusion cross-section of LCP ($\sigma_{fus}$), we have chosen in the fragmentation potential profile the $^2$H, $^3$H, and $^{4,5,6}$He LCP for both mic and mac T.B.E. cases.

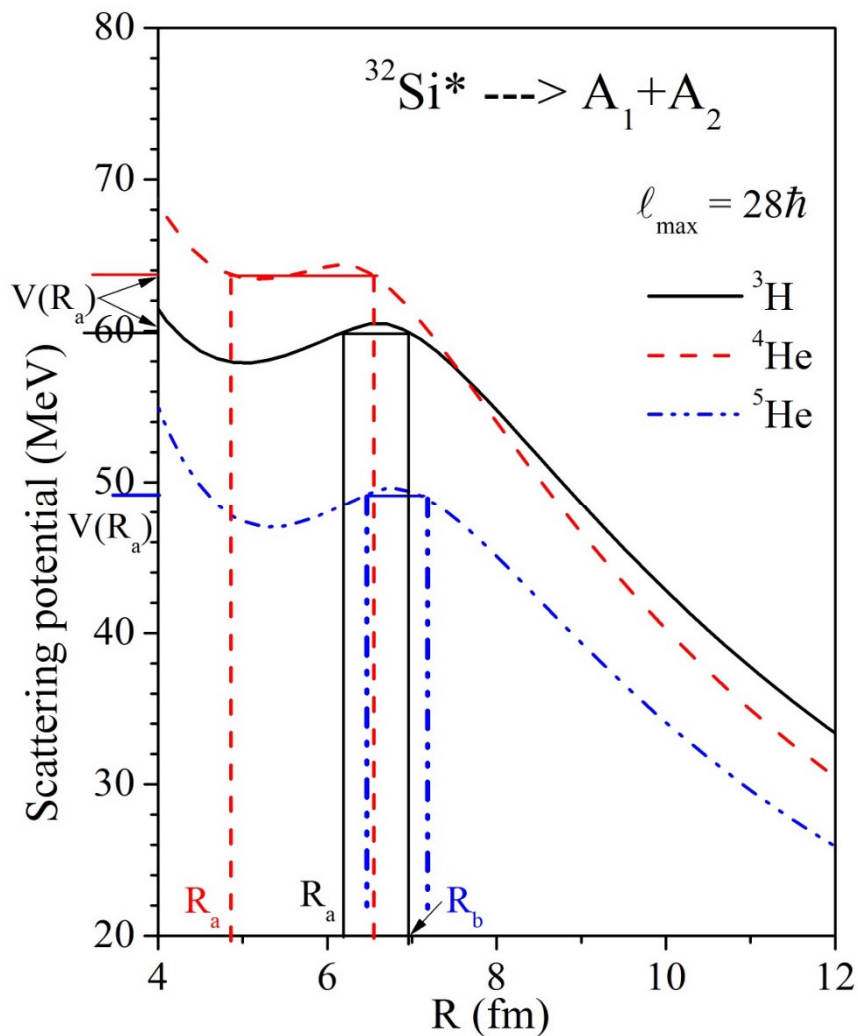FIG. 6. Scattering potential for the emission of $^3$H, $^4$He, $^5$He in the decay of $^{32}$Si$^*$ nuclear system at $T = 3.09$ MeV.

➤ The barrier is lowest for $^5$He compared to $^3$H, $^4$He channels. It may be due to the centrifugal effect, since the angular momentum-dependent potential is high for lighter $^3$H and $^4$He channels.

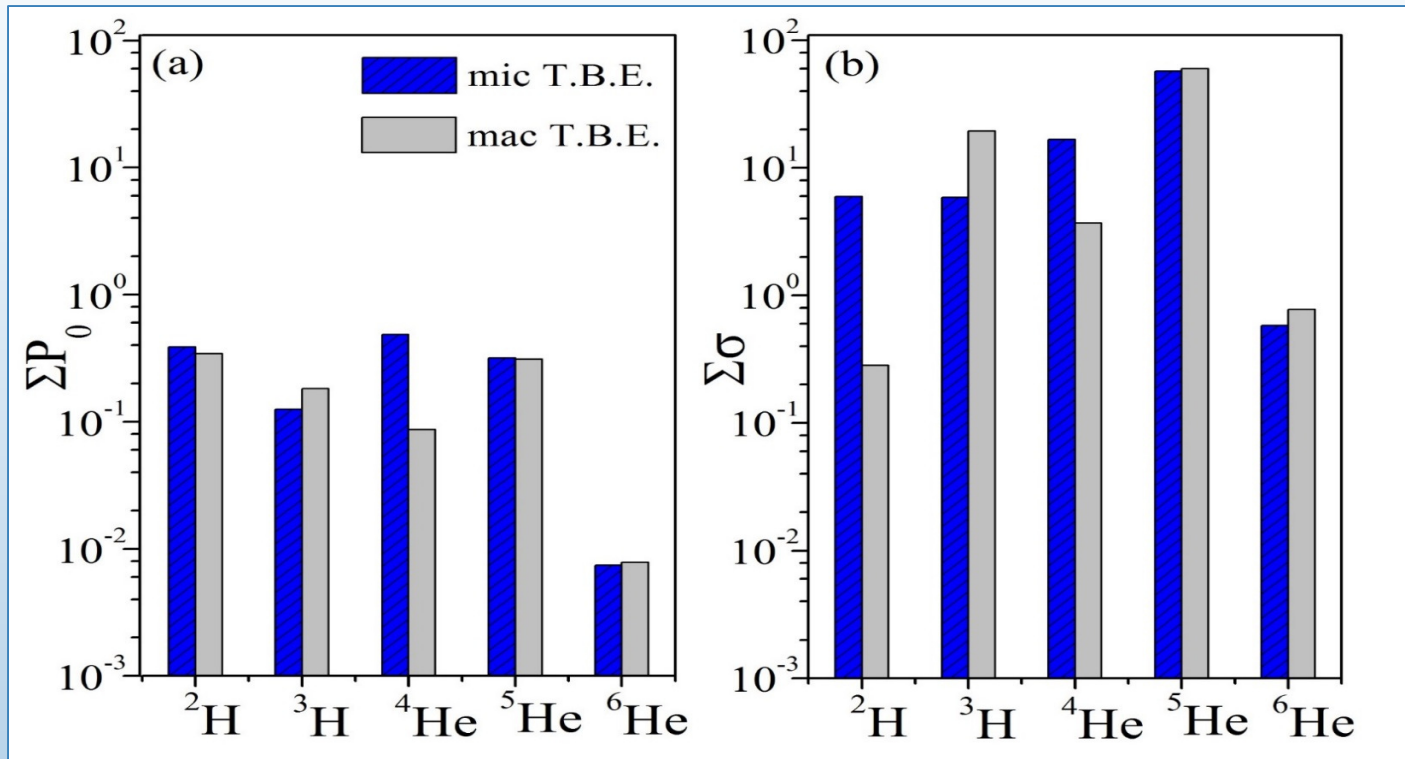➤ Among $^4$He and $^5$He channels, the Coulomb barrier is reduced for n-rich $^5$He.

FIG. 7. (a) Summed up preformation probability $\Sigma P_0$ and (b) summed up cross-section $\Sigma\sigma$ of different LCP channels in the decay of $^{32}$Si* nuclear system formed at T = 3.09 using mac and mic T.B.E.

❖ $P_0$ of $^4$He is considerably larger in case of mic T.B.E. compared to mac T.B.E. case whereas for $^5$He and $^6$He the value of $P_0$ is approximately same for both cases of T.B.E.

❖ For mic T.B.E case, the contribution of $^2$H and $^4$He channels is relatively enhanced while than of $^3$H channel is low compared to the case of mac T.B.E.

❖ $^5$He is the major contributor in $\sigma_{fus}$ for both mac and mic T.B.E. cases. It is probably due to the low barrier for $^5$He leading to higher P through interaction barrier, compared to other LCP channels. It is in line with statistical EVAPOR model calculations.

❖ It is evident that trend in $\sigma$ is due to $P_0$ signifying that nuclear structure information is carried by $P_0$ and the cross-sections follow the trend of $P_0$ for mic and mac T.B.E. choices.

TABLE I: The fusion cross-section associated with light charge particles (LCP) in $^{20}O + ^{12}C$ reaction calculated within DCM using macroscopic (mac) and microscopic (mic) T-dependent binding energies (T.B.E.) from Davidson formula and using RMF theory, respectively, along with comparison with other model results and experimental data [9].

| $E_{c.m.}$ | $T$ | mac T.B.E. | | | mic T.B.E. | | | $\sigma_{fus}^{Bass}$ | $\sigma_{fus}^{TDHF}$ | $\sigma_{fus}^{Expt}$ |
|---|---|---|---|---|---|---|---|---|---|---|
| | | $\ell_{max}$ | $\sigma(A_i)$ | $\sigma_{fus}^{DCM}$ | $\ell_{max}$ | $\sigma(A_i)$ | $\sigma_{fus}^{DCM}$ | | | |
| (MeV) | (MeV) | $(\hbar)$ | (mb) | (mb) | $(\hbar)$ | (mb) | (mb) | (mb) | (mb) | (mb) |
| 7.35 | 3.09 | 28 | $\sigma_{2H}=0.28$ $\sigma_{3H}=19.48$ $\sigma_{4He}=3.70$ $\sigma_{5He}=60.0$ $\sigma_{6He}=0.78$ | 84.2 | 27 | $\sigma_{2H}=5.96$ $\sigma_{3H}=5.87$ $\sigma_{4He}=16.72$ $\sigma_{5He}=57.35$ $\sigma_{6He}=0.58$ | 86.5 | 1.8 | 24.2 | 82.3±26 |
| 9.29 | 3.18 | 28 | $\sigma_{2H}=0.30$ $\sigma_{3H}=39.56$ $\sigma_{4He}=4.20$ $\sigma_{5He}=82.31$ $\sigma_{6He}=0.82$ | 127.6 | 27 | $\sigma_{2H}=1.96$ $\sigma_{3H}=12.88$ $\sigma_{4He}=26.81$ $\sigma_{5He}=77.31$ $\sigma_{6He}=0.96$ | 119.6 | 59 | 92.2 | 133.4±37 |

➢ At higher $E_{c.m.}$, the contribution of $^2H$ channel decreases than at $E_{c.m.} = 7.35$ MeV while the contribution of $^3H$ channel increases at higher $E_{c.m}$, in accordance with statistical EVAPOR model results.

➢ The DCM calculated fusion cross-sections are in good agreement with the experimental data.

# Conclusion

➢ The structure and magnitude of fragmentation potential are found to change notably along with a change in energetically favored fragments with inculcation of RMF theory-based mic T.B.E.

➢ The $\alpha$ and $\alpha$-like fragment are favored energetically at all $\ell$-values for the mic T.B.E. case in line with statistical EVAPOR model results whereas only neutrons are preformed at lower $\ell$-values for mac T.B.E.

➢ This change in the nuclear structure embodied via fragmentation potential energy carries its imprints in the preformation probability $P_0$ of different fragments and affects the contribution of individual light-charged particle (LCP) channel in the $\sigma_{\text{fus}}$.

➢ The inculcation of mic T.B.E. predict/give a significant contribution of the $^4$He in the $\sigma_{\text{fus}}$ associated with LCP and $^5$He is the dominant LCP channel contributing in $\sigma_{\text{fus}}$.

➢ The Bass model and TDHF model under predict the fusion cross-section associated with LCP emission whereas DCM-calculated $\sigma_{\text{fus}}$ are in good agreement with the available experimental data.

# Acknowledgements

➢ Prof. Suresh K. Patra, IOP, Bhubaneswar
➢ Prof. BirBikram Singh, Akal University, Talwandi Sabo
➢ Organizers of NSP-2021